THE JOURNAL OF PHYSICAL CHEMISTRY C

ARTICLE

pubs.acs.org/JPCC

Rh-Decorated Cu Alloy Catalyst for Improved C_2 Oxygenate Formation from Syngas

Yong-Hui Zhao,† Ming-Mei Yang,† Dapeng Sun, Hai-Yan Su,* Keju Sun, Xiufang Ma, Xinhe Bao, and Wei-Xue Li*

State Key Laboratory of Catalysis, Dalian Institute of Chemical Physics, Chinese Academy of Science, Dalian 116023, China

Supporting Information

ABSTRACT: C_2 oxygenate (acetaldehyde, ethanol, etc.) formation from syngas (CO + H_2) is an important industrial process for the production of clean liquid energy fuels and valuable chemical feedstocks that are catalyzed industrially by Rh modified with Mn and Fe, etc. In an effort to identify catalysts based on less expensive metals and higher C_2 oxygenate selectivity, density functional theory (DFT) calculations were performed to tune the relative activity of the selectivity-determining steps, i.e., CO insertion in CH_x (x = 1, 2, 3) versus CH_x hydrogenation by changing composition and structure of material. We find that the Rh-decorated Cu alloy catalyst has significantly lower CO insertion barriers compared to pristine Rh(111) and vicinal Rh(553) surfaces, whereas the variation of CH_x hydrogenation barriers on the three surfaces is modest. A semiquantitative kinetic analysis based on DFT calculations shows that the C_2 oxygenate selectivity on RhCu(111) is substantially improved, with the production rate of C_2 oxygenates slightly higher than CH_4 under experimental conditions, compared with Rh(111) and Rh(553) that are highly selective to CH_4. Our calculations suggest that the improved C_2 oxygenate selectivity on the RhCu alloy is primarily due to the fact that CO insertion is rather sensitive, whereas hydrogenation is insensitive to the ensemble effect. Furthermore, the Rh-decorated Cu alloy has stronger resistance toward coking and lower constituent cost compared to pure Rh catalysts and is thus a promising candidate for an improved C_2 oxygenate synthesis catalyst.

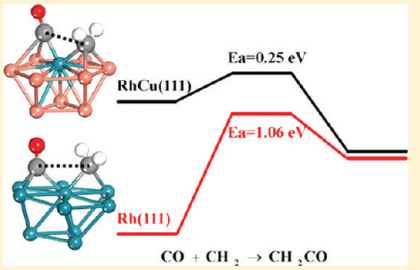

1. INTRODUCTION

Formation of C_2 oxygenates (typically referred to as acetaldehyde, ethanol, etc.) from syngas (CO + H_2) is an important industrial process for the production of clean liquid energy fuels and valuable chemical feedstocks.[1−4] The chemical process involves an intricate reaction network composed of a number of surface intermediates and competing elementary reaction pathways. Rhodium-based catalysts modified with the transition metals Mn and Fe, etc., are often used industrially.[5−17] This system leaves ample room for improvement, particularly in terms of C_2 oxygenate selectivity and price. The design of catalytically selective and inexpensive materials for C_2 oxygenate formation will require insight into the structure of catalysts combined with an understanding of the relation between composition and structure of catalysts and reactivity. On the basis of density functional theory calculations, we demonstrated in this paper a strategy of fabricating an inexpensive Rh-decorated Cu alloy to tune the relative activity of the key elementary steps that determine the selectivity toward C_2 oxygenates.

To date, there is no generally accepted mechanism available for C_2 oxygenate formation.[18] One possible route involves a key intermediate, i.e., surface hydrocarbon species (CH_x), produced by CO dissociation followed by hydrogenation (carbide mechanism), or vice versa (hydrogen-assisted CO dissociation mechanism), which then undergo (i) hydrogenation/dehydrogenation to produce CH_4 or coking and (ii) chain growth either by CO insertion in CH_x monomer, or by carbene coupling, or by condensation of C1-oxygenates with elimination of water, leading to the formation of C_n($n \geq 2$)-oxygenates or hydrocarbons.[10,19,20] Recently, our DFT calculations show that HCO insertion is superior and/or competitive to CO insertion and carbene coupling for chain growth on Rh and Co catalysts.[21] In addition, without C−O bond breaking, CO can hydrogenate gradually to produce methanol. The product selectivity is controlled by the capabilities of catalysts to perform hydrogenation/dehydrogenation and chain growth.[3,12,22,23] On the basis of DFT calculations, Liu et al. found that CH_3 is the most favorable monomer among all the CH_x species, and the selectivity to ethanol on Rh(111) is controlled by methane formation by CH_3 hydrogenation and C−C bond formation by CO insertion in methyl species.[24] They suggest that the iron promoters, which can suppress methane formation and/or boost C−C bond formation, are indispensable to achieve high productivity and selectivity for ethanol. However, Kapur et al. show that CH_2 is the most favored monomer among all the CH_x species, and CO insertion into CH_2 is deduced to be the precursor for C_2 oxygenate formation.[25] Considering the discrepancy about CH_x monomer formation in these two studies, we extend the

Received: May 27, 2011
Revised: August 9, 2011
Published: August 10, 2011

selectivity-controlling steps to be CO insertion in CH_x and CH_x hydrogenation (x = 1−3). The challenge for improved C_2 oxygenates selectivity is thus to tune the relative activity of CO insertion in CH_x and CH_x hydrogenation by changing the composition and structure of catalysts. Later on we perform our own calculations for the competitive CH_2 and CH_3 monomer formation. Herein, we only focus on the CO insertion for chain growth. Since HCO insertion is superior and/or competitive with respect to CO insertion,[21] the selectivity with respect to the C_2 oxygenates obtained might be underestimated.

In general, CH_x (x = 1−3), CO, and H species are the key intermediates related to the elementary steps that are critical to C_2 oxygenate selectivity, i.e., CO insertion in CH_x (C_2 oxygenates) and CH_x hydrogenation (CH_4). It has been reported that CO insertion and CH_x hydrogenation exhibit a similar feature: CH_x moves relatively little in reaction processes due to the extremely strong adsorption on Rh, Ru, and Pd catalysts.[24−28] This means that CH_x activation contributes little to the CH_x hydrogenation and CO insertion barriers, and it would be insensitive to composition and structure of catalysts. Instead, the CO and H activation have a pronounced contribution to the CO insertion and CH_x hydrogenation barriers. Furthermore, H activation in many hydrogenation reactions does not exhibit strong dependence on composition and structure of catalysts.[26−28] Therefore, one approach to tune the relative barriers of CH_x hydrogenation and CO insertion is via modification of CO activation through ensemble effect and/or ligand effect by alloying or decreasing the size of catalyst.

The previous DFT studies indicate that the addition of a group IB metal such as Cu to group VIII metals (Rh, Pd) can largely vary CO binding energy at different adsorption sites which is related to CO activation.[29−31] In this paper, Rh is occupied as the essential component of the catalyst since it exhibits the best performance toward C_2 oxygenate formation, and Cu is used as a second metal to modify the CO activation. Experimentally, phase diagrams of the Cu−Rh binary alloy showed that these two metals were partially miscible and formed two alloy phases, i.e., a rhodium-rich phase and a copper-rich phase, at T < 1400 K.[32] Sinfelt et al. studied the cluster formation on Rh−Cu/SiO_2 bimetallic samples by the extended X-ray absorption fine structure (EXAFS) technique and found an apparent enrichment of copper on the surface but little miscibility in the bulk of Rh−Cu clusters.[33] The Rh−Cu/SiO_2 catalyst has been reported as an efficient system for NO reduction by CO, the conversion of methane to ethane, and some dehydrogenation reactions.[34−36] In addition, adsorbate activation and product selectivity can be largely tuned on step or kinks. Arakawa et al. have reported an increase in CO turnover frequency (TOF) for syngas conversion as the silica-supported Rh nanoparticle size increases from 2 to 6 nm. CH_3OH is formed selectively on small particles (<2 nm), while methane and acetaldehyde (CH_3CHO) are favored on large (∼6 nm) nanoparticles. Medium-sized particles (∼2−3.5 nm) correspond to maximum selectivity for CH_3CH_2OH.[37] The size effect on the selectivity was studied recently by density functional theory calculation on Mn-doped Rh clusters.[17]

In this paper, density functional calculations were performed to tune the relative activity of the selectivity-controlling steps, i.e., CO insertion in CH_x and CH_x hydrogenation by changing composition and physical structure of catalysts. We find that the Rh-decorated Cu alloy catalyst has significantly lower CO insertion barriers compared to pristine Rh(111) and vicinal Rh(553) surfaces, whereas the variation of CH_x hydrogenation barriers on the three surfaces is modest. A semiquantitative kinetic analysis based on DFT calculations shows that the C_2 oxygenate selectivity on RhCu(111) is substantially improved, with the production rate of C_2 oxygenates slightly higher than CH_4 under typical experimental conditions, compared with Rh(111) and Rh(553) that are highly selective to CH_4. Our calculations suggest that the improved C_2 oxygenate selectivity on the RhCu alloy is primarily due to the fact that CO is rather sensitive, whereas H is insensitive to ensemble effects at initial states of CO insertion and CH_x hydrogenation steps. Furthermore, the Rh-decorated Cu alloy has stronger resistance toward coking and lower constituent cost compared to pure Rh catalysts. Because these reactions, i.e., CO activation and hydrogenation of carbon-containing species, are prototypical reactions for many other catalytic systems, the results presented here are of general interest.

2. COMPUTATIONAL DETAILS

In our studies, we use the Vienna ab initio simulation package (VASP)[38,39] with projector-augmented wave potentials[40,41] and the generalized gradient approximation (PW91) for the exchange correlation functional.[42] The PAW projectors provided in VASP were employed, and a plane-wave cutoff energy of 400 eV was used in all calculations. The calculated lattice constant for bulk Rh is 3.84 Å, which agrees well with the experimental value (3.80 Å),[43] and has been employed throughout the present paper.

For the flat surface, a five-layer Rh(111)−(2 × 2) slab (corresponding to 0.25 ML of surface coverage), periodically repeated in a super cell geometry with vacuum region of 15 Å between any two successive metal slabs, was used to simulate the surface. The surface Brillouin zone was sampled by a (4 × 4 × 1) Monkhorst−Pack grid.[44] Adsorptions were allowed only on one of the two exposed surfaces. The chemisorbed species and the atoms in the top two metal layers were fully relaxed until the residual forces were less than 0.03 eV/ Å, while the remaining atoms were fixed in their bulk-truncated positions. Spin-polarized calculations for isolated molecules and atoms were carried out in a (15 Å × 15.25 Å × 15.5 Å) unit cell with a single K point. The stepped Rh(553) surface was modeled by a slab with five equivalent Rh(111) layers. We chose a (2 × 1) unit cell containing two step atoms. These slabs were separated by a 15 Å vacuum in the z-direction. The uppermost two layers parallel to the (111) terrace and the adsorbates were allowed to relax until the residual forces were less than 0.03 eV/Å. For the stepped surfaces, the Brillouin zone integration was performed using a (4 × 2 × 1) Monkhorst−Pack grid. To study the alloy effect on a Rh catalyst, a quarter of surface atoms in Cu(111) is substituted by Rh atoms; this surface will henceforth be referred to as RhCu(111). All other parameters are the same as for the Rh(111) surface. All parameters defining the numerical accuracy of the calculations were carefully tested and well converged.

In the present work, the binding energy E_b was defined as the energy gain upon adsorption with respect to the clean substrates and corresponding species in the gas phase. Here a negative (positive) value indicates that the adsorption is exothermic (endothermic). Transition states (TSs) were located by a constrained minimization method,[45,46] and the relaxations were stopped if the residual forces were less than 0.03 eV/Å. TSs of some of the elementary reactions were also searched by the climbing-image nudged elastic band method (CI−NEB).[47,48] The results show that the TS found by the former method provides sufficient accuracy for the surface chemical reactions studied as the latter do.

3. ANALYSIS OF CO INSERTION VERSUS CH_X HYDROGENATION ON RH(111)

As mentioned in the Introduction, surface hydrocarbon species (CH_x) are a key intermediate for syngas conversion, which undergo sequential hydrogenation to produce CH_4 or CO insertion followed by hydrogenation to produce C_2 oxygenates such as ethanol, acetaldehyde, etc. The previous DFT studies indicate that the production of C_2 oxygenates and CH_4 should be largely controlled by the CO insertion and CH_x hydrogenation steps.[24,25]

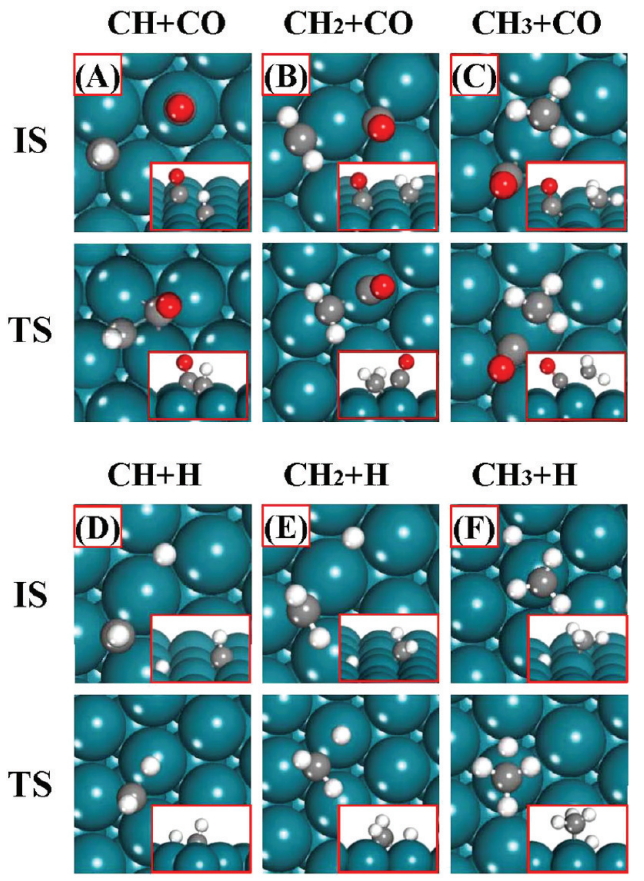

Figure 1. Top and side view (insets) of the initial state (IS, left column) and the transition state (TS, right column) of CO insertion and CH_x hydrogenation in CH_x (x = 1,2,3) on Rh(111). Dark cyan, gray, red, and white spheres represent Rh, C, O, and H atoms, respectively.

Aiming to provide insight into C_2 oxygenate selectivity, we first investigate the competitive CO insertion in CH_x and CH_x hydrogenation (x = 1−3) steps on Rh(111). Two main features can be found from the most favorable structures at the initial states and transition states for CH_x hydrogenation and CO insertion on Rh(111), as shown in the schematics in Figure 1. (1) A specific CH_x species exhibits similar structure at the initial state of CH_x hydrogenation and CO insertion in CH_x, and the geometry of CH_x changes little during the reaction processes. For instance, CH and CH_3 bind through their C end at hcp-hollow (Figure 1A, 1D) and top sites (Figure 1C, 1F) at all the ISs and TSs regardless of the hydrogenation and CO insertion reactions. This can be due to the fact that Rh(111) binds CH_x species (CH, CH_2) significantly stronger than CO and H, with the order of −6.81 eV/CH > −4.25 eV/CH_2 > −1.93 eV/CH_3 ∼ −1.93 eV/CO > −0.58 eV/H as listed in Table 1(for structures see Figure S1 in Supporting Information). (2) CO/H adsorbs on the hollow site at the IS and moves to the top site, sharing one metal atom with CH_x at the TS of CO insertion and CH_x hydrogenation, with the exception of CO insertion of CH, where CO sits at the top site originally and moves to the bridge site at the TS. These features imply that CH_x activation contributes little; instead, the CO and H activation has a pronounced contribution to CH_x hydrogenation and CO insertion barriers E_{act} on Rh(111).

The activation energy barriers for CO insertion in CH, CH_2, and CH_3 are calculated to be 1.01, 1.06, and 1.20 eV, respectively, significantly higher than the corresponding hydrogenation barriers of 0.61, 0.48, and 0.45 eV. The energetic and geometric information at the TSs is listed in Table 2, and the energy profile is shown in Figure 4A. Our calculations indicate that Rh(111) is highly selective for CH_4 rather than C_2 oxygenates regardless of the CH_x monomer. These results agree well with experimental studies and previous DFT studies.[24,49] To quantitatively analyze activation energy E_{act}, we use a convenient approach presented by Hammer, originally for NO dissociation on metal surfaces.[50] In this model, the adsorption energy of reactants A and B at the

Table 1. Adsorption Energies (E_{ads}) and Geometrical Configurations of the Most Stable State of Various Surface Species on Rh(111), RhCu(111), and Rh(553) Surfaces[a]

	Rh(111)		RhCu(111)		Rh(553)	
species	E_{ads} (eV)	site	E_{ads} (eV)	site	E_{ads} (eV)	site
C	−7.29	hcp	−6.03	fcc-(RhCuCu)[c]	−7.59	near-step-corner
H	−0.58	fcc	−0.44	hcp-(RhCuCu)[c]	−0.55	near-step-fcc
CO	−1.93	top	−2.01	top-(Rh)	−1.95	step-top
CH	−6.81	hcp	−5.78	fcc-(RhCuCu)[c]	−6.76	near-step-fcc
CH_2	−4.25	hcp	−3.60	bri-(Rh,Cu)[c]	−4.46	step-bri
CH_3	−1.93	fcc	−1.86	top-(Rh)	−2.00	near-step-fcc
CH_4	−0.03	top	−0.08	top-(Rh)	−0.07	near-step-top
CHCO	−3.38	$\eta_2\mu_3$-(C,C^b)	−2.80	$\eta_2\mu_3$-($C_{Rh,Cu}C_{Rh}$[d])	−3.51	near step-$\eta_2\mu_3$(CC^b)
CH_2CO	−1.40	$\eta_2\mu_3\nu_2$(CC^bO^b)	−1.21	$\eta_2\mu_2$-($C_{Rh}C_{Rh}$[d])	−1.56	near step-$\eta_2\mu_2\nu_2$(CC^bO^b)
CH_3CO	−2.49	$\eta_2\mu_2$(CO^b)	−2.15	$\eta_2\mu_1$-(C_{Rh}[d])	−2.78	near step-$\eta_2\mu_2$(CO^b)

[a] The nomenclature $\eta_i\mu_j\nu_k$(CCO) is used to designate that the two C and O atoms of the adsorbate are bonded to i, j, and k metal atoms on the surface. [b] Is the C of the CO (carbonyl) end. [c] Is the hollow site surrounded by the atoms in parentheses. [d] C_{Rh} is the C of the CO end, coordinated with a Rh atom on RhCu(111).

dx.doi.org/10.1021/jp204961g |J. Phys. Chem. C 2011, 115, 18247–18256

Table 2. Calculated Structural Parameters at the Transition States, Prefactors A (s^{-1}) of CH_x (x = 1,2,3) Hydrogenation and CO Insertion at 543 K, and Activation Energies and Reaction Energies of the Forward (E_a and ΔE) and Reverse Reactions (in eV), Respectively

	Rh(111)			RhCu(111)			Rh(553)		
reactions	$d_{C-H/C}$	A	$E_a(\Delta E)$	$d_{C-H/C}$	A	$E_a(\Delta E)$	$d_{C-H/C}$	A	$E_a(\Delta E)$
C + H → CH	1.65		0.60(−0.49)	1.69		0.48(−0.93)	2.75		0.36(0.24)
CH + H → CH_2	1.48	1.39×10^{13}	0.61(0.54)	1.58	2.07×10^{13}	0.47(0.04)	1.55	1.19×10^{13}	0.55(0.20)
CH_2 + H → CH_3	1.61	7.59×10^{12}	0.48(0.09)	1.72	1.72×10^{13}	0.29(−0.56)	1.64	1.26×10^{13}	0.47(0.30)
CH_3 + H → CH_4	1.53	1.53×10^{13}	0.45(−0.23)	1.59	1.11×10^{13}	0.28(−0.44)	1.59	5.31×10^{12}	0.60(0.06)
CH + CO → CHCO	1.70	2.31×10^{13}	1.01(0.81)	1.82	2.10×10^{13}	0.72(0.05)	1.69	1.71×10^{13}	1.30(0.96)
CH_2 + CO → CH_2CO	1.83	7.40×10^{12}	1.06(0.67)	1.97	1.15×10^{13}	0.25(−0.44)	1.79	1.21×10^{13}	0.91(0.77)
CH_3 + CO → CH_3CO	1.87	8.62×10^{12}	1.20(−0.01)	1.92	1.08×10^{13}	0.53(−0.18)	1.88	9.25×10^{11}	0.82(0.02)

TS, E^{TS}, is decomposed into the rebonding energy of the separated A and B fragments in the TS geometry, $E^{TS}_{ads}(A)$ and $E^{TS}_{ads}(B)$, respectively, and the interaction energy (E^{TS}_{int}) between A and B moieties

$$E^{TS} = E^{TS}_{ads}(A) + E^{TS}_{ads}(B) + E^{TS}_{int} \quad (1)$$

Similarly, for the initial state we obtain

$$E^{IS} = E^{IS}_{ads}(A) + E^{IS}_{ads}(B) + E^{IS}_{int} \quad (2)$$

Hence the activation energy E_{act} is derived easily as a function of the variations of the rebonding and the adsorption energy summed over the fragments $\Delta\Sigma E_{ads}$ and the variations of the interaction energy ΔE_{int}, between the initial and the transition states

$$E_{act} = E^{TS} - E^{IS} = \Delta E_{ads}(A) + \Delta E_{ads}(B) + \Delta E_{int} \quad (3)$$

Using the barrier decomposition scheme, the energy cost for CH_x activation ΔE_{ads} (CH_x) in CO insertion of CH_x is calculated to be 0.13 eV (x = 1), 0.28 eV (x = 2), and 0.55 eV (x = 3), as shown in Figure 5A and Table S1 (Supporting Information). Compared to the corresponding CO insertion barriers of 1.02, 1.06, and 1.20 eV, the contribution of CH_x activation is small. Likewise, CH_x activation has a small contribution, i.e., 0.07(x = 1), 0.04(x = 2), and 0.12 eV(x = 3), to CH_x hydrogenation barriers of 0.61, 0.47, and 0.45 eV (see Figure 5B and Table S2, Supporting Information). Instead, CO, particularly H activation, contributes reasonably to CO insertion and CH_x hydrogenation barriers. For instance, the energy cost of H activation is 0.34 (x = 1) and 0.35 eV (x = 2), which consists of a large portion of corresponding CH_x hydrogenation barriers (0.61 and 0.47 eV). This can be ascribed to the larger energy cost for H moving than CO moving from a hollow site (IS) to a top site (TS). Additionally, the differences of interaction energy of reactants between IS and TS, ΔE_{int}, are significant, which also make a large contribution to the activation energy of the CO insertion and hydrogenation steps. This is because the two reactants now share bonding with a metal atom at the TSs. The so-called bonding competition effect will reduce the reactant chemisorption energies and thus increase the interaction energy.[51] It has been shown that the bonding competition effect is determined by the reactant and metal valency.[27] As the adsorbate valency decreases, the E_{int} decreases, and this rationalizes well why CO insertion in CH_x has a larger E_{int} than CH_x hydrogenation.

Having analyzed the energetics and geometry of CO insertion in CH_x and CH_x hydrogenation on Rh(111), we now demonstrate the strategy of tuning the relative reaction barriers of these competitive steps. As discussed above, CH_x moves relatively little in reaction processes due to the extremely strong adsorption on transition metal surfaces. This means that CH_x activation contributes little to the CH_x hydrogenation and CO insertion barriers, and it would be insensitive to composition and structure of catalysts. Instead, CO and H moving from a hollow site (IS) to a top site (TS) has a pronounced contribution to CO insertion and CH_x hydrogenation barriers. It has been reported that H activation in many hydrogenation processes does not exhibit strong dependence on composition and structure of catalysts.[26−28] Therefore, the enhancement in C_2 oxygenate selectivity can be achieved through modification of CO activation. It can be seen clearly from Figure 1B and 1D that CO adsorption at the initial state involves an ensemble of three metal atoms (with the exception of coadsorption with CH as shown in Figure 1A). At the transition state, CO moves to the top site (see Figure 1A, 1B, and 1C), where the ligand effect could be applied to tune the relative stability. The insight can be used to design an optimal catalyst for C_2 oxygenates formation, that is, to substantially destabilize CO at the initial state compared to the transition state through ensemble effect and/or ligand effect by alloying or decreasing the size of catalyst which will be explored below. Finally, the interaction energy variation, ΔE_{int}, is significant, which also makes a large contribution to the activation energy of the CO insertion and hydrogenation steps. To tune the relative ΔE_{int} for CO insertion and CH_x hydrogenation is desirable but not discussed in the present paper.

4. EFFECT OF COMPOSITION AND STRUCTURE ON CO INSERTION AND CH_X HYDROGENATION

4.1. Effect of Composition. As discussed above, two factors determine the suitability of a surface as a catalyst for selective C_2 oxygenate formation: the ability of the surface to destabilize CO at the initial state and/or that of the surface to stabilize CO at the transition state of CO insertion in CH_x steps. One approach to achieve this goal is to take advantage of the ensemble effect by alloying the reactive and inert atoms, which should be significant in destabilizing CO at the hollow site at the IS. While at the TS CO moves to the top site of a reactive metal atom, with CO binding largely stabilized compared to the IS, it has been shown that the addition of a group IB metal such as Cu to group VIII

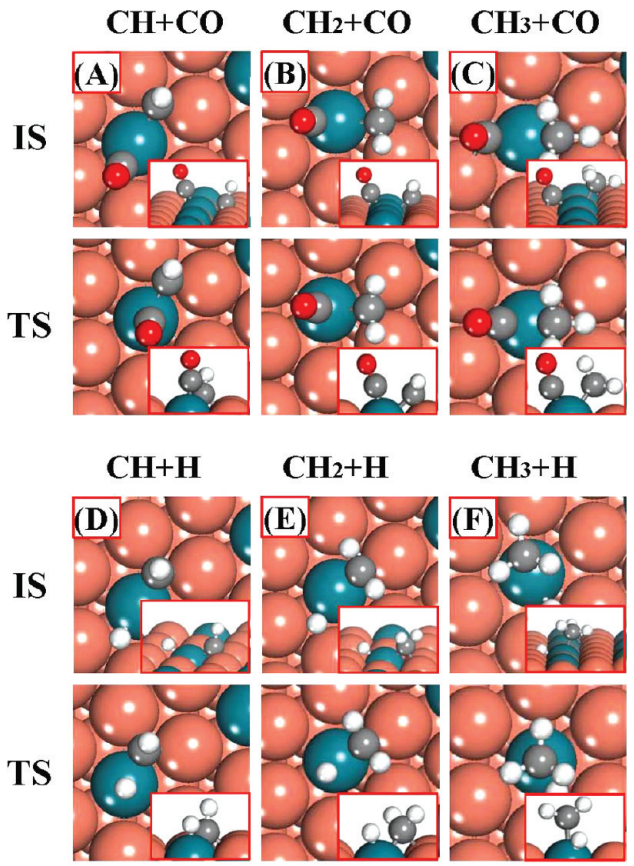

Figure 2. Top and side view (insets) of the initial state (IS, left column) and the transition state (TS, right column) of CO insertion and CH_x hydrogenation in CH_x(x = 1,2,3) on RhCu(111). Dark cyan, dark salmon, gray, red, and white spheres represent Rh, Cu, C, O, and H atoms, respectively.

metals (Rh and Pd) can largely vary CO binding energy at different adsorption sites which is related to CO activation.[29,30] In this paper, Rh is occupied as the essential component of the catalyst since it exhibits the best performance toward C_2 oxygenate formation, and Cu is used as a second metal to modify the CO activation. We fabricate a Cu-rich (Rh-decorated Cu) alloy, with 25% of the Cu atoms substituted by Rh in the outmost Cu layer of the Cu(111) slab, which could ensure CO coordination with both reactive Rh and inert Cu atoms at the IS. At the same time, the Rh decorated Cu alloy binds CO at the top site of Rh atoms, leading to large stabilization at the TS (see Figure 2A, 2B, and 2C), thereby fulfilling the two requirements for improved C_2 oxygenates selectivity.

To destabilize CO that coordinated to the reactive Rh atom and inert Cu atoms at the IS and stabilize CO at the top site of Rh atom at the TS, one premise is that the ligand effect is less significant than the ensemble effect on RhCu(111). On atomic dispersion in the top layer of a Cu(111) substrate, the ligands of the Rh atoms are different from those on the Rh(111) surface. The ligand effect induced by the less reactive Cu atoms causes an upshift in the d-band center of surface Rh atoms by 0.54 eV, when compared with the Rh atoms in the top layer of a Rh(111) surface. Upshifting the d-band center of a surface tends to increase the interaction strength of the surface with adsorbates.[52] This can be verified by the variation in the binding energies of adsorbates sitting at the top site of Rh atoms, such as CO (0.08 eV) and CH_4 (0.05 eV), between Rh(111) and RhCu(111), as listed in Table 1. However, the increase is small, meaning that the contribution of ligand effect to adsorbates binding is modest. On the other hand, if an adsorbate interacts with an ensemble of reactive Rh and inert Cu atoms, the ensemble effect can weaken adsorbate binding on the RhCu(111) surface.[30] As listed in Table 1, the adsorbate binding can be significantly destabilized with the coordination of Cu atoms compared to Rh(111). For instance, CH_2 binding at the bridge site of Rh and Cu atoms (coordinated with one Cu atom, see Figure S1(e), Supporting Information) is destabilized by 0.65 eV, whereas the destabilization is doubled for C (1.26 eV) and CH (1.03 eV) at the hollow site of Rh and Cu atoms (coordinated with two Cu atoms, see Figure S1(a) and S1(d), Supporting Information). This weakened binding of adsorbates can be ascribed to a combination of the ligand and ensemble effects. Since the ligand effect strengthens adsorbate binding on the RhCu(111) surface and the magnitude is modest, the ensemble effect is dominant in tuning the reactivity of RhCu(111). For large C_2 oxygenate molecules, the site preference is changed between Rh(111) and RhCu(111) (see Figure S1(h), S1(i), and S1(j), Supporting Information), and it is therefore difficult to measure the ligand effect and ensemble effect. However, we note that CHCO binding with both Rh and Cu atoms has a decrease in adsorption energy by 0.58 eV compared to Rh(111), more than that for CH_2CO (0.19 eV) and CH_3CO (0.34 eV) binding only with Rh atoms. A destabilization of adsorbates due to the ensemble effect can also be clearly seen.

As expected, H does not exhibit strong dependence on the composition of the catalyst. The ensemble effect for H adsorption on RhCu(111) is modest, with the decrease of H adsorption energy by 0.14 eV compared to pure Rh(111). For CO adsorption on RhCu(111), when by itself, CO prefers to adsorb at the top site of the Rh atom (see Figure S1(c), Supporting Information). The CO adsorbed on the hollow site of Rh and Cu atoms would slide off into the adjacent top site of the Rh atom, suggesting it is not a true minimum in the potential energy surface. When coadsorbed with CH_x, CO prefers to move to a hollow site of Rh and Cu atoms, and the destabilized CO binding by the ensemble effect at the IS of CO insertion in CH_x can be expected (see Figure 2A, 2B, and 2C, energy decomposition is shown below), which leads to more facile CO insertion steps as listed in Table 2. We found that the barriers to CO insertion in CH_x on RhCu(111) are substantially lower than on Rh(111) by 0.29 eV(x = 1), 0.81 eV(x = 2), and 0.67 eV(x = 3). However, the CH_x hydrogenation reactions are only slightly affected, with the decrease in the activation energies between the two surfaces by 0.14, 0.19, and 0.17 eV, respectively. The barrier difference between CO insertion in CH_x and CH_x hydrogenation on RhCu(111) is greatly lowered, with the values of 0.25, −0.04, and 0.25 eV. Note that the energy barrier of CO insertion in CH_2 is even slightly lower than that of CH_2 hydrogenation. Moreover, CO insertion in CH_x on Rh-decorated Cu alloy becomes neutral or exothermic, with reaction energies of 0.05 eV(x = 1), −0.44 eV(x = 2), and −0.18 eV(x = 3). Compared to pure Rh(111), which is endothermic or neutral by 0.81, 0.67, and −0.01 eV, the RhCu alloy is more favorable for CO insertion in CH_x on thermodynamic grounds.

Note that the lateral interaction may have an influence on the CO insertion in CH_x and CH_x hydrogenation reaction. We studied CH_2 + H and CH_2 + CO on Rh(111) and RhCu(111)

surfaces in the (3 × 3) unit cell. Calculated barriers for CH_2 + H and CH_2 + CO are 0.46 and 0.45 eV on RhCu(111) and 0.37 and 1.11 eV on Rh(111), respectively. For comparison, calculated barriers for CH_2 + H and CH_2 + CO in the (2 × 2) unit cell are 0.29 and 0.25 eV on RhCu(111) and 0.48 and 1.06 eV on Rh(111), respectively. It is clear that though the lateral interaction using a smaller (2 × 2) cell may slightly decrease the absolute values of the activation barriers, the selectivity of CO insertion, and hydrogenation the main point addressed in the manuscript has not been affected. This is understandable since the effect of the lateral interaction on the selectivity has been largely canceled out.

The barrier decomposition for CO insertion in CH_x on RhCu(111) can be seen in Figure 4A. A striking feature is that CO activation gains energy on RhCu(111), whereas it costs energy on Rh(111) regardless of CO insertion in CH_x pathways. This rebonding energy variation of CO, ΔE_{ads}(CO), decreases between Rh(111) (0.15−0.37 eV) and RhCu surface (−0.07 ∼ −0.22 eV, see Table S1, Supporting Information), hence revealing the stabilizing effect of copper. By comparison with Rh(111), the gain of −0.57 (x = 1), −0.33 (x = 2), and −0.44 eV (x = 3) for ΔE_{ads}(CO) in CO insertion of CH_x on RhCu(111) corresponds greatly to the reduction of the barrier of 0.29, 0.81, and 0.67 eV. In addition, the decrease in energy cost for CH_x activation (0.05−0.27 eV) and the interaction energy variation ΔE_{int} (0.2 eV for x = 2, 3; see Table S1, Supporting Information) also have an additional contribution to the lowering of the activation barriers on RhCu(111) with respect to Rh(111). An exception is the interaction energy variation ΔE_{int} for CO insertion in CH, having an increase of 0.36 eV on RhCu(111) compared to Rh(111), thereby leading to the smaller decrease in energy barrier (0.29 eV) between Rh(111) and RhCu(111) than CO insertion of CH_2 and CH_3 (0.81 and 0.67 eV). Among all the CO insertion in CH_x pathways, RhCu(111) exhibits the most effective tuning for CO insertion in CH_2. The lowering of the energy barrier (0.81 eV) between Rh(111) and RhCu(111) results from the decrease(increase) in energy cost(gain) for CH_x activation (0.29 eV), CO activation (0.33 eV), and the interaction energy variation ΔE_{int} (0.2 eV).

For CH_x hydrogenation pathways, CH_x exhibits a quasi-constant variation of the rebonding energy between Rh(111) and RhCu(111) surfaces, with the energy difference of 0.03 eV for CH hydrogenation at most (see Figure 4B). The lowering of the activation barrier on RhCu(111) with respect to Rh(111) is primarily a result of the decrease in rebonding energy variation for H activation (x = 1, 2) or the decrease in the variation of the interaction energy ΔE_{int} (x = 3). By comparison with Rh(111), the energy gain of −0.14 and −0.18 eV (see Table S2, Supporting Information) for ΔE_{ads}(H) and ΔE_{int} on RhCu(111) corresponds exactly to the reduction of the CH and CH_3 hydrogenation barriers. However, the values are small, indicating that H activation and the interaction energy variation do not seem to be intrinsic to a given metallic substrate.

The energetic and geometric analysis show that the enhanced CO insertion in CH_x is achieved through modification of the CO activation by the ensemble effect on the Rh-decorated Cu alloy. This ensemble effect significantly destabilizes CO at the initial state, compared to the transition state where only ligand effect is available. At the same time, H activation is insensitive to the ensemble effect, leading to the improved selectivity of CO insertion over CH_x hydrogenation.

It is interesting to compare the pure Cu catalyst, which is active and selective for methanol formation, and the present Rh-decorated Cu catalyst. We calculated CH_x + CO and CH_x + H (x = 1,2,3) on Cu(111) and found that the barriers obtained are essentially the same as those on RhCu(111) (not shown here). In particular, the results indicate again that CH_2 + CO has higher activity than CH_2 + H hydrogenation on Cu(111). Namely, though CH_x coordinates with the Rh atom on RhCu(111) and the Cu atom on Cu(111), there is no pronounced activation for CH_x during the CO insertion of CH_x and CH_x hydrogenation reaction and therefore no influence on the activation and competition between CO insertion and hydrogenation on RhCu(111) and Cu (111), as discussed above. However, pure Cu alone is unreactive for C═O bond breaking and CH_x formation, which is necessary for production of C2 oxygenates.

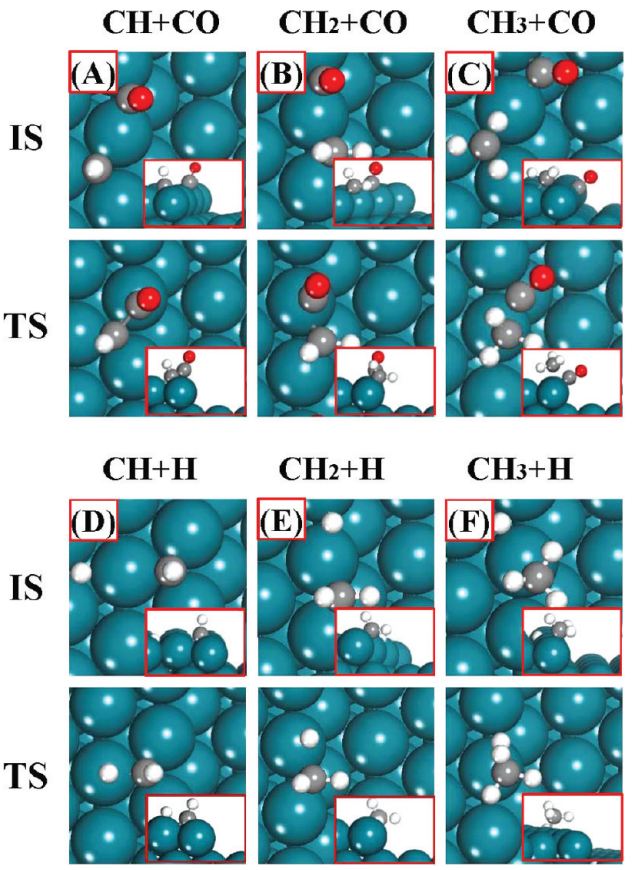

Figure 3. Top and side view (insets) of the initial state (IS, left column) and the transition state (TS, right column) of CO insertion and CH_x hydrogenation in CH_x(x = 1,2,3) on Rh(553). Dark cyan, gray, red, and white spheres represent Rh, C, O, and H atoms, respectively.

4.2. Effect of Structure. Having discussed the effect of composition on C_2 oxygenate selectivity, we are now in a position to investigate the effect of structure, specifically the presence of a step edge. We first studied various species adsorption in several high-symmetry sites on Rh(553). For simplicity, only the binding energies at the most stable sites are listed in Table 1 (except CO where binding at top sites is listed due to inaccuracies in the DFT treatment of CO adsorption), and the structures are shown in Figure S1 (Supporting Information). In general, the vicinal Rh(553) surface binds the adsorbates quasi-degenerately or stronger compared to Rh(111), with the largest increase in binding energy (0.3 eV) found for atomic C adsorption. The reason is that the coordination number (CN) of the

surface atoms is lower in the vicinal Rh(553) than in Rh(111) (CN = 7 vs CN = 9), resulting in a smaller bandwidth, higher energy of the *d* band center (−1.49 eV/Rh(553) vs −1.76 eV/Rh(111)), and hence higher reactivity. Among them, CO does not exhibit strong site preferences on Rh(553). Two configurations with binding energies differing by 0.04 eV are found; an atop state at the step has a binding energy of −1.95 eV (see Table 1), and a bridge state at the step has a binding energy of −1.99 eV. The binding energies of CO on Rh(553) are very similar to those on Rh(111) (−1.93 eV/top, −2.00 eV/hcp). Likewise, binding of gas-phase atomic H at the fcc site near the step (−0.55 eV) is quasi-degenerate to that on Rh(111). Our results agree well with previous DFT studies by Kupur and coworkers.[25] These results suggest that the vicinal Rh(553) would not play an effective role in modifying the CO and H activation.

Compared to RhCu(111) that enhances all the CO insertion and CH_x hydrogenation steps by ensemble effect, the effect of the presence of a step edge is more complicated. As listed in Table 2, Rh(553) slightly enhances the CH_x hydrogenation (x = 1, 2) and CO insertion in CH_2, whereas it largely accelerates the CO insertion in CH_3, with the decrease in energy barrier of 0.01−0.15 and 0.36 eV compared to Rh(111). This can be assigned to the geometrical and electronic effect induced by the stepped Rh(553), where the two fragments of the reaction can both be stabilized without "shared" metal atoms at the transition state (see Figure 3C). The larger enhancement in CO insertion in CH_3 may be due to the fact that CH_3 moves from the hollow site to the top site in the hydrogenation process, which leads to the decrease in ΔE_{int} and hence additional energy gain. For CH_3 hydrogenation and CO insertion of CH, the energy barriers on Rh(553) are increased compared to Rh(111), which can be ascribed to a larger stabilization at the IS than at the TS (Figure 3F and 3A). As a result, the difference in barrier between CO insertion in CH and CH hydrogenation increases from 0.40 eV on Rh(111) to 0.75 eV on Rh(553). For CO insertion and hydrogenation of CH_2 (Figure 3B and 3E), the barrier difference is decreased to 0.44 eV on Rh(553), compared to 0.58 eV on Rh(111). Among all the pathways, CH_3 provides the most possible pathway, with a markedly decreased barrier difference of 0.22 eV, compared with 0.75 eV on Rh(111). These results mean that Rh(553) enhances the formation of C_2 oxygenates relative to CH_4 formation through the CH_2 and CH_3 monomer. However, the improvement on Rh(553) is modest, compared to RhCu(111).

5. DISCUSSIONS

5.1. Selectivity of C_2 Oxygenates versus CH_4. To compare the competitive C_2 oxygenates and CH_4 formation, we defined the so-called relative selectivity as the proportion of the corresponding rate constants for CO insertion in CH_x (C_2 oxygenates) and CH_x hydrogenation (CH_4) $k_{(CHx+CO)}/(k_{(CHx+CO)} + k_{(CHx+H)})$. The coverage of CO is suggested to be higher than that of H on the Rh surface under typical experimental conditions (P_{CO} = 4 atm, P_{H2} = 8 atm, and T = 523−623 K).[24] Therefore, the relative C_2 oxygenate selectivity should be higher than the present analysis. Detailed information about prefactors calculation is given in the Supporting Information. Using the prefactors and reaction barriers listed in Table 2, we calculate the rate constants k for each CO insertion and CH_x hydrogenation step and the relative selectivity at various temperatures. We emphasize that the selectivity discussed in this section is the relative selectivity for CO insertion versus hydrogenation of CH_x-(x = 1,2,3), instead of the overall selectivity for the methane formation and oxygenates.

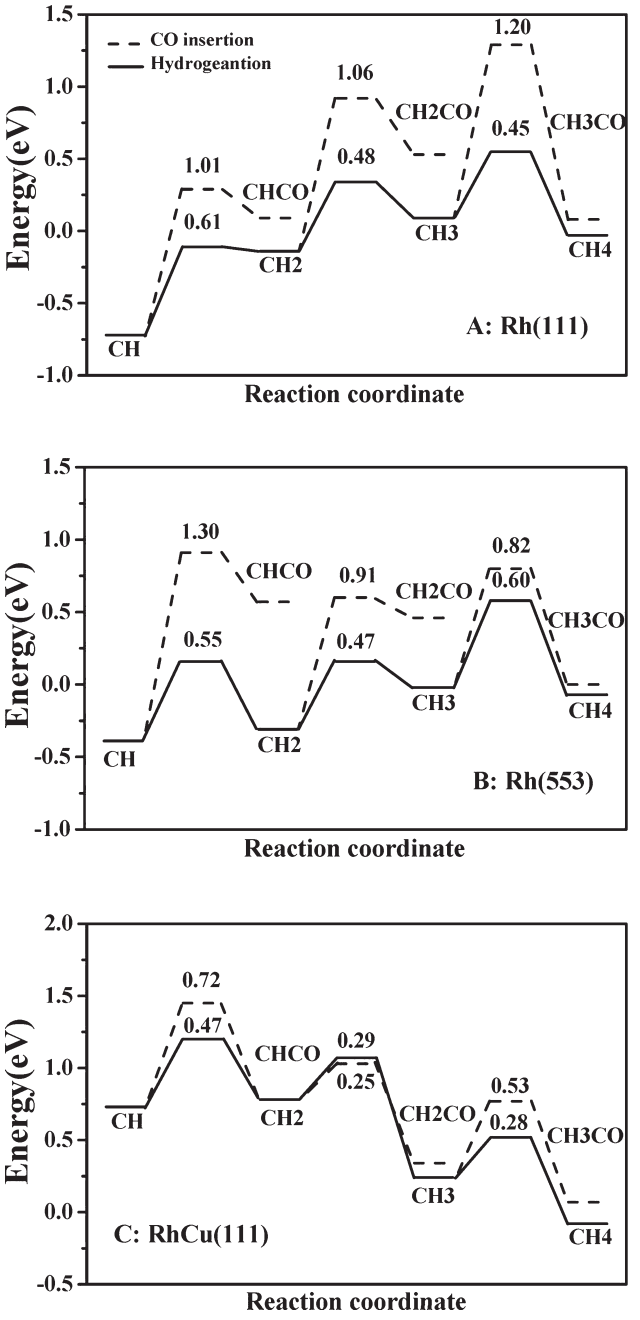

Figure 4. Calculated barriers and reaction energies for CH_x(x = 1,2,3) hydrogenation and CO insertion in CH_x on Rh(111) (A), Rh(553) (B), and RhCu(111) (C). All energies are referenced to CH_4 in the gas phase.

The relative selectivity of CHCO and CH_2, produced by CO insertion in CH and CH hydrogenation, on Rh(111), Rh(553), and RhCu(111), is shown in Figure S2 (Supporting Information). It is clear that for temperatures ranging from 200 to 800 K the hydrogenation process (CH + H → CH_2) is dominant on all three surfaces, and the relative selectivity toward CHCO is near zero. A slight increase of CHCO selectivity on the RhCu(111) surface should be noticed here (see Figure S2(c), Supporting Information), which primarily originates from the

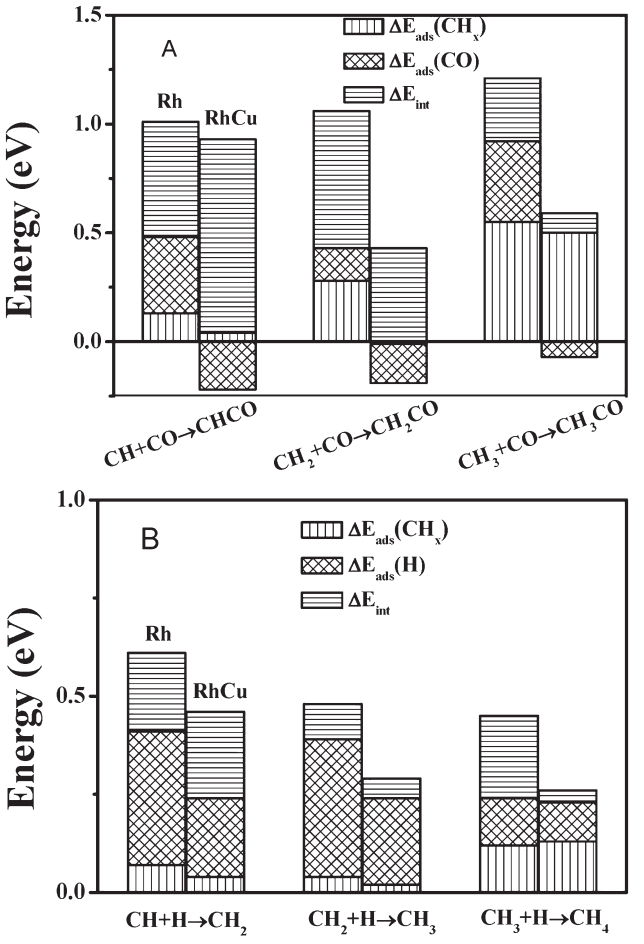

Figure 5. Barrier decomposition analysis of the CO insertion in CH_x (A) and CH_x hydrogenation (B) on Rh(111) and RhCu(111) surfaces. The gray, dark yellow, and olive columns represent the variations of the interaction energy ΔE_{int}, the variations of the rebonding energy of CO/H ($\Delta E_{ads}(CO)/\Delta E_{ads}(H)$), and CH_x($\Delta E_{ads}(CH_x)$) between the initial and the transition states and (also see Table 2) as defined in the paper.

largely decreased barrier difference between the two competitive reaction steps compared with the other two surfaces, as shown above in Sections 3 and 4.

The relative selectivity of CH_2CO ($CH_2 + CO \rightarrow CH_2CO$) and CH_3 ($CH_2 + H \rightarrow CH_3$) on the three surfaces is shown in Figure 6. It can be seen clearly that in the temperature range 200−800 K the hydrogenation process is dominant on both Rh(111) and Rh(553) (see Figure 6A and 6B). However, the CO insertion in CH_2 becomes dominant: the selectivity order toward CH_2CO and CH_3 is inversed on the RhCu(111) surface at low temperatures (Figure 6C). With increasing temperature, the proportion of CH_2CO drops, while the proportion of CH_3 increases gradually. Under the typical experimental conditions (T = 523−623 K), the selectivity of C_2 oxygenates is slightly higher than that of CH_3. This substantially improved selectivity of CH_2CO here gives an indication of the unique property of the RhCu(111) surface compared with the other two surfaces. The selectivity of CH_3CO ($CH_3 + CO \rightarrow CH_3CO$) and CH_4 ($CH_3 + H \rightarrow CH_4$) on the three different surfaces is shown in Figure S3 (Supporting Information). The results are similar to what has been found for CH_2 and CHCO as shown above, thus no more depiction here.

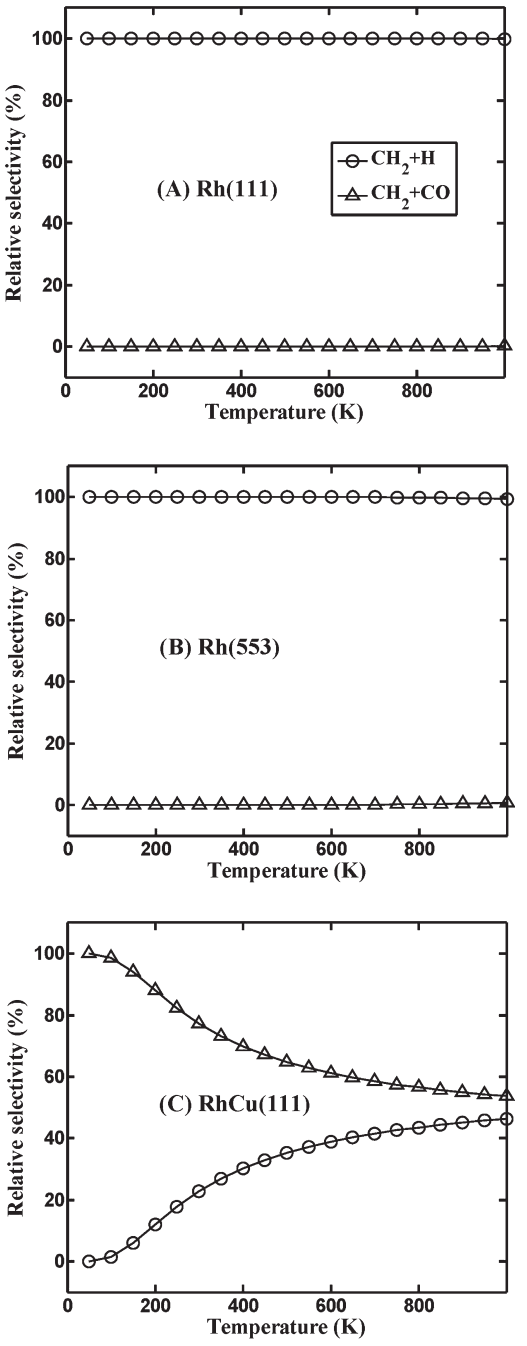

Figure 6. Temperature dependence of the relative selectivity of CH_2 hydrogenation versus CO insertion in CH_2 on Rh(111) (A), Rh(553) (B), and RhCu(111) (C) (for details see Supporting Information).

The above results show clearly that compared to Rh(111) and Rh(553) the relative selectivity of CO insertion with CH_x(x = 1, 2, 3) on RhCu(111) has been improved in general, and particularly for CH_2 + CO. Moreover, as seen in Figure 4, the barrier for either CH_2 + CO or CH_2 + H on RhCu(111) is lower than that of CH_2 dehydrogenation. This indicates that corresponding CH_2 concentration should be rather high, which is important for CO insertion and high C_2-oxygenate selectivity.

5.2. Analysis of CH_x Dehydrogenation on Rh(111), Rh(553), and RhCu(111). The potential energy surface in Figure 4 involves all the elementary reaction steps for CO insertion in

CH_x ($x = 1-3$) and CH_x hydrogenation on Rh(111), Rh(553), and RhCu(111). In this section, we focus on the reverse reaction of CH_x hydrogenation, i.e., CH_x dehydrogenation processes that related to the carbon deposition. It can be seen from Table 2 and Figure 4 that CH_x dehydrogenation on Rh(111) has two main features: (1) The first dehydrogenation step $CH_4 \rightarrow CH_3 + H$ has a high activation energy barrier (0.68 eV). Once the first C−H bond scission occurs, the sequential hydrogen abstraction from the resulting CH_3 intermediate is quite facile, with the barrier of 0.39 eV for $CH_3 \rightarrow CH_2 + H$ and 0.07 eV for $CH_2 \rightarrow CH + H$. However, the last dehydrogenation step $CH \rightarrow C + H$ is hindered by a high barrier of 1.09 eV. (2) CH_x dehydrogenation is either modestly endothermic, with the reaction energy of 0.23 eV for $CH_4 \rightarrow CH_3 + H$ and 0.49 eV for $CH \rightarrow C + H$, or slightly/modestly exothermic by −0.09 eV for $CH_3 \rightarrow CH_2 + H$ and −0.54 eV for $CH_2 \rightarrow CH + H$. These results indicate that the last dehydrogenation step $CH \rightarrow C + H$ is the rate-limiting step for carbon formation.

Compared to pure Rh(111), the activation energy barrier for each dehydrogenation step on RhCu(111) is increased by 0.04∼0.48 eV (see Table 2). In particular, the last dehydrogenation step $CH \rightarrow C + H$, which is the rate-limiting step for carbon formation, has an activation energy barrier of 1.41 eV on RhCu(111), largely higher than the corresponding barrier of 1.09 eV on Rh(111). Moreover, CH_x dehydrogenation on RhCu(111) is either modestly/strongly endothermic, with the reaction energy of 0.44 eV for $CH_4 \rightarrow CH_3 + H$, 0.56 eV for $CH_3 \rightarrow CH_2 + H$, and 0.93 eV for $CH \rightarrow C + H$, or neutral by −0.04 eV for $CH_2 \rightarrow CH + H$. These results mean that the carbon formation is unfavorable thermodynamically and kinetically. Additionally, the CH_x, particularly CH, which blocks the active sites on Rh(111), binds much weaker on RhCu(111), and hence the probability toward coking can be largely decreased. Interestingly, the activation energy barriers for CH_x dehydrogenation on Rh(553) are very small, in the region of 0.17∼0.54 eV. The activation energy barrier of the last dehydrogenation step ($CH \rightarrow C + H$) is only 0.12 eV, and the first dehydrogenation step $CH_4 \rightarrow CH_3 + H$ (0.54 eV) turns out to be the rate-limiting step for carbon formation. Furthermore, all the CH_x dehydrogenation steps on Rh(553) are neutral or modestly exothermic. These results show that Rh(553) has a larger possibility toward coking compared to Rh(111).

Our calculations show that the formation energy of Rh-decorated Cu(111) is nearly neutral. Moreover, we find that the Rh-decorated Cu alloy with Rh in the top layer is favored over that with Rh in the subsurface or bulk. The driven force is the lower surface energy and larger atomic size of Rh than Cu atoms. This suggests that the synthesis of the material is possible. Experimentally, the SiO_2-supported copper-rich RhCu surface alloy phase has been indeed observed.[53] In syngas conversion conditions, where the reductive atmosphere is dominant, the highly Rh dispersed in the top layer of Cu can also be more stable due to the stronger Rh−CO binding compared to Cu−CO binding. The present work suggests that the Rh-decorated Cu alloy has an improved selectivity toward C_2 oxygenates over CH_4 formation, stronger resistance to coking, and lower constituent cost compared to pure Rh catalysts and is thus a promising candidate for an improved C_2 oxygenate synthesis catalyst. The understanding of the ensemble effect in tuning catalytic reaction performance at the atomic level can potentially be used to develop and design improved catalysts for C_2 oxygenate synthesis and other important reactions of interest.

Under realistic conditions of syngas conversion, the presence of coadsorbed atoms/molecules such as surface oxygen, hydroxyl, and water etc. on the catalysts may have a significant influence on the binding of intermediates, even for preferred reaction paths. Quantitative investigations into the effect of coadsorbed species with extensive theoretical calculations would be desirable, but this is beyond the scope of the present work.

6. CONCLUSIONS

In summary, CO insertion in CH_x and CH_x hydrogenation on Rh(111), Rh(553), and RhCu(111) has been studied using DFT calculations in an effort to provide atomic level insight into selectivity control for C_2 oxygenates synthesis. We find that compared to Rh(111) which has the activation energy difference of 0.4 eV($x = 1$), 0.58 eV($x = 2$), and 0.75 eV($x = 3$) between CO insertion and CH_x hydrogenation the novel Rh-decorated Cu alloy substantially decreases the values to 0.25, −0.04, and 0.25 eV. However, Rh(553) does not exhibit a significant enhancement of CO insertion relative to hydrogenation steps. A semiquantitative kinetic analysis based on DFT derived parameters shows that the C_2 oxygenate selectivity on RhCu(111) is substantially improved, with the production rate of C_2 oxygenates slightly higher than CH_4 under experimental conditions, compared with Rh(111) and Rh(553) that are highly selective to CH_4. The improved C_2 oxygenate selectivity on RhCu(111) is primarily achieved through the ensemble effect, which largely destabilizes CO relative to H at the initial state of CO insertion in CH_x and CH_x hydrogenation steps, thereby accelerating the CO insertion reaction relative to CH_x hydrogenation. Furthermore, the Rh-decorated Cu alloy has stronger resistance toward carbon deposition and lower constituent cost compared to pure Rh catalysts and is thus a promising candidate for an improved C_2 oxygenate synthesis catalyst.

■ ASSOCIATED CONTENT

Supporting Information. Detailed information on the structure of adsorbates, the semiquantitative kinetic analysis, relative selectivity of CH_x hydrogenation versus CO insertion in CH_x ($x = 1, 3$), and energetic analysis. This material is available free of charge via the Internet at http://pubs.acs.org.

■ AUTHOR INFORMATION

Corresponding Author

*E-mail: wxli@dicp.ac.cn; hysu@dicp.ac.cn.

Author Contributions

†These authors contributed equally to this work.

■ ACKNOWLEDGMENT

We thank finical support by the Natural Foundation of Science of China (Grants 20873142, 20733008, 20923001) and the Ministry of Science and Technology of China (Grants 2007CB815205, 2011CB932704).

■ REFERENCES

(1) Anderson, R. B. *Fischer−Tropsch and Related Synthesis*; Academic Press: New York, 1983.
(2) Mill, G. A. E.; E., E. *CHEMTECH* **1989**, *19*, 626.
(3) Chuang, S. C. G.; J., G.; Wender, I. *J. Catal.* **1985**, *95*, 435.

(4) Pan, X. L.; Fan, Z. L.; Chen, W.; Ding, Y. J.; Luo, H. Y.; Bao, X. H. *Nat. Mater.* **2007**, *6*, 507.
(5) Bhasin, M. M. B.; W., J.; Ellgen, P. C.; Wilson, T. P. *J. Catal.* **1978**, *54*, 120.
(6) Burch, R. P.; M, I. *Appl. Catal.* **1992**, *88*, 39.
(7) Gao, J. M.; H., X.; Chien, A. C. Y.; Torres, W.; Goodwin, J. G. *J. Catal.* **2009**, *262*, 119.
(8) Gysling, H. J. M.; R., J.; Apai, G. *J. Catal.* **1987**, *103*, 407.
(9) Haider, M. A. G.; M., R.; Davis, R. J. *J. Catal.* **2009**, *261*, 9.
(10) Ichikawa, M.; Fukushima, T. *J. Phys. Chem.* **1985**, *89*, 1564.
(11) Kesraoui, S. O.; R.; Blackmond, D. G. *J. Catal.* **1987**, *105*, 432.
(12) Kip, B. J. H.; E., G. F.; Prins, R. *Appl. Catal.* **1987**, *35*, 141.
(13) Nakajo, T.; Sano, K. I.; Matsuhira, S.; Arafawa, H. *J. Chem. Soc., Chem. Commun.* **1987**, *9*, 647.
(14) Ma, X. F.; Deng, H. Q.; Yang, M. M.; Li, W. X. *J. Chem. Phys.* **2008**, 129.
(15) Yang, M. M.; Bao, X. H.; Li, W. X. *J. Chem. Phys.* **2007**, *127*, 024705.
(16) Yang, M. M.; Bao, X. H.; Li, W. X. *J. Phys. Chem. C* **2007**, *111*, 7403.
(17) Mei, D.; Rousseau, R.; Kathmann, S. M.; Glezakou, V.-A.; Engelhard, M. H.; Jiang, W.; Wang, C.; Gerber, M. A.; White, J. F.; Stevens, D. J. *J. Catal.* **2010**, *271*, 325.
(18) Gao, J.; Mo, X. H.; Goodwin, J. G. *J. Catal.* **2010**, *275*, 211.
(19) Chuang, S. S. C. S.; R., W.; Khatri, R., Jr. *Top. Catal.* **2005**, *32*, 225.
(20) Efstathiou, A. M. C.; T.; Bianchi, D.; Bennett, C. O. *J. Catal.* **1994**, *148*, 224.
(21) Zhao, Y. H. S.; K., J.; Ma, X. F.; Liu, J. X.; Sun, D. P.; Su, H. Y.; Li, W. X. *Angew. Chem., Int. Ed.* **2011**, *50*, 5335.
(22) Biloen, P. S.; W., M. H. *Adv. Catal.* **1985**, *30*, 165.
(23) Dry, M. E. *Catal. Sci. Technol.* **1981**, *1*, 159.
(24) Choi, Y. M.; Liu, P. *J. Am. Chem. Soc.* **2009**, *131*, 13054.
(25) Kapur, N.; Hyun, J.; Shan, B.; Nicholas, J. B.; Cho, K. *J. Phys. Chem. C* **2010**, *114*, 10171.
(26) Liu, Z. P.; Hu, P. *J. Chem. Phys.* **2001**, *115*, 4977.
(27) Liu, Z. P.; Hu, P. *J. Am. Chem. Soc.* **2003**, *125*, 1958.
(28) Michaelides, A.; Hu, P. *J. Chem. Phys.* **2001**, *114*, 5792.
(29) Gonzalez, S.; Sousa, C.; Illas, F. *Surf. Sci.* **2003**, *531*, 39.
(30) Lopez, N.; Norskov, J. K. *Surf. Sci.* **2001**, *477*, 59.
(31) Gupta, M. S.; Smith, M. L.; Spivey, J. J. *ACS Catal.* **2011**, *1*, 641.
(32) Massalski, T. B., Okamoto, H.; Subramanian, P. R.; Kacprazak, L. *Binary Alloy Phase Diagrams*, 2nd ed.; ASM International: Ohio, 1992.
(33) Meitzner, G.; Via, G. H.; Lytle, F. W.; Sinfelt, J. H. *J. Chem. Phys.* **1983**, *78*, 882.
(34) Petrov, L.; Soria, J.; Dimitrov, L.; Cataluna, R.; Spasov, L.; Dimitrov, P. *Appl. Catal., B* **1996**, *8*, 9.
(35) Reyes, P.; Pecchi, G.; Fierro, J. L. G. *Langmuir* **2001**, *17*, 522.
(36) Solymosi, F.; Cserenyi, J. *Catal. Lett.* **1995**, *34*, 343.
(37) Arakawa, H.; Takeuchi, K.; Matsuzaki, T.; Sugi, Y. *Chem. Lett.* **1984**, 1607.
(38) Kresse, G. H. *J. Phys. Rev. B: Condens. Matter* **1993**, *48*, 13115.
(39) Kresse, G. F. *J. Phys. Rev. B: Condens. Matter* **1996**, *54*, 11169.
(40) Blöchl, P. E. *Phys. Rev. B: Condens. Matter* **1994**, *50*, 17953.
(41) Kresse, G. J.; D. *Phys. Rev. B: Condens. Mater* **1999**, *59*, 1758.
(42) Perdew, J. P. C.; J., A.; Vosko, S. H.; Jackson, K., A.; Pederson, M. R.; Singh, D. J.; Fiolhais, C. *Phys. Rev. B: Condens. Matter* **1992**, *46*, 6671.
(43) Birgersson, M. A.; C., O.; Borg, M.; Andersen, J. N. *Phys. Rev. B: Condens. Matter* **2003**, *67*, 045402.
(44) Monkhorst, H. J.; Pack, J. D. *Phys. Rev. B* **1976**, *13*, 5188.
(45) Abashkin, Y.; Russo, N. *J. Chem. Phys.* **1994**, *100*, 4477.
(46) Abashkin, Y.; Russo, N.; Toscano, M. *Theor. Chim. Acta* **1995**, *91*, 179.
(47) Henkelman, G.; Jonsson, H. *J. Chem. Phys.* **2000**, *113*, 9978.
(48) Henkelman, G.; Uberuaga, B. P.; Jonsson, H. *J. Chem. Phys.* **2000**, *113*, 9901.
(49) Spivey, J. J.; Egbebi, A. *Chem. Soc. Rev.* **2007**, *36*, 1514.
(50) Hammer, B. *Surf. Sci.* **2000**, *459*, 323.
(51) Liu, Z. P.; Hu, P. *J. Am. Chem. Soc.* **2001**, *123*, 12596.
(52) Mavrikakis, M.; Hammer, B.; Norskov, J. K. *Phys. Rev. Lett.* **1998**, *81*, 2819.
(53) Irons, L.; Mini, S.; Brower, W. E. *Mater. Sci. Eng.* **1988**, *98*, 309.